9A.4 SPECTRAL IDENTIFICATION AND SUPPRESSION OF GROUND CLUTTER CONTRIBUTIONS FOR PHASED ARRAY RADAR

Svetlana Bachmann*, Dusan Zrnic, and Chris Curtis
Cooperative Institute for Mesoscale Meteorological Studies, University of Oklahoma and
NOAA/OAR National Severe Storm Laboratory, Norman, Oklahoma

1. INTRODUCTION

When a radar beam is pointing at a low elevation angle, it illuminates a large portion of the ground. This results in the detection of strong echoes referred as ground clutter (GC), which obscure echoes from the atmosphere. In radar meteorology this problem is known as ground clutter contamination. Spectral ground clutter filters (GCF) are widely used to identify and remove the contributions from GC in the frequency domain (Torres 1998, Siggia and Passarelli 2004, Golden 2005, Hubbert et al. 2006, Ice et al. 2007, Bachman and Zrnic 2007). Generally, spectral filters are applied only for the resolution volumes that are indicated by the ground clutter map. A clutter map can be obtained from the power returns in clear air conditions, from *dc* power, or using a more sophisticated scheme such as the clutter mitigation decision (CMD) algorithm (Hubbert et al. 2006) that uses fuzzy logic on several fields (texture of reflectivity, reflectivity gradient and clutter phase alignment). Once the resolution volumes with clutter are flagged by the map, a variety of spectral GCF can be applied. Among the simplest GCF are the notch filters. Gaussian model adaptive processing (GMAP) is an evolved GCF that performs an iterative fit of a Gaussian model to the spectral coefficients containing clutter contribution to the Doppler spectrum (Siggia and Passarelli 2004, Ice et al. 2007).

Occasionally GC maps are not available such as when the radar is brought up at a new location. Often GC maps are outdated due to erection of new structures such as cranes or towers near the established sites. Sometimes GC maps are not accurate due to storms that have damaged the trees and structures or have deposited icicles on the structures and power lines. Even an accurate GC map becomes vague in atmospheric conditions that cause abnormal radar beam propagation (lower or higher than normal, abnormal beam bending, etc.). In such cases the radar moments (power, velocity, and spectral width) contain errors that most likely propagate into the radar related products and models. While these errors can sometimes be quite obvious, they can also be concealed within the acquired radar display. GC with small relative power is not filtered at all (US DoC 2006). Such clutter might be negligible if one is dealing with a strong storm, but becomes significant if the signal of interest is a weak clear-air echo or arises from a small non-cooperative aircraft. Thus, in a wide variety of important practical scenarios, static clutter maps prove totally inadequate as the basis of an optimal GCF solution.

With a mechanically steered antenna, the azimuth angle of the antenna advances slightly with respect to the ground clutter map during the acquisition of a single resolution volume – as a consequence of the continuous rotation of the antenna. While minute, this angular advancement nevertheless alters the GC contributions to the composite Doppler spectrum over the course of the resolution volume. This effect is known as *smearing*. In a phased array system, smearing does not occur because the electronically steered beam can dwell at a static azimuth and elevation throughout the acquisition of a resolution volume. This is an important fact that motivates an entirely new approach to spectral filtering applicable to both phased arrays and mechanically steered radars.

In this paper, we introduce new techniques for identification of the intrinsic GC contribution to the radar spectrum. Instead of a two-step process comprising *a priori* clutter map generation and subsequent application of GCF at the time of data acquisition, we here propose a one-step spectral filter applied everywhere without the need for a clutter map. We use the phase rather than the power of the complex radar signal for identification. We partition the raw radar signal into two subsequences consisting of the samples with even and with odd indices (*i.e.*, a two-phase polyphase decomposition) and we compute the complex spectra of these two subsequences. The spectral density of the differential phase between these two spectra, which we shall refer to as $\phi_{DP\text{-}EO}$, is central to our proposed GCF algorithm. Where the intrinsic $\phi_{DP\text{-}EO}$ is observed near zero, the corresponding contributions to the radar power spectrum are due to GC. The number of such coefficients is usually small, and their location in the Doppler spectrum is not necessarily symmetric. In this paper, we present spectral fields with notched zero-$\phi_{DP\text{-}EO}$ coefficients to enhance visual clarity. We provide illustrative displays of moments obtained from these notch-filtered spectral fields which show that the weather echoes are preserved while the GC and *dc* are removed. Our examples show no evidence of the zero isodop (the artifact that appears in power displays in storms at zero Doppler velocity due to GCF). A simple linear interpolation of the spectral coefficients adjacent to the notch can be used if

* *Corresponding author address*: Svetlana Bachmann, University of Oklahoma, CIMMS, Norman, OK 73072;

e-mail: svetlana.bachmann@noaa.gov

desired. The proposed technique does not require clutter maps.

2. METHODOLOGY

Here, we define $\phi_{DP\text{-}EO}$ as the intrinsic spectral density of differential phase between the complex spectral coefficients of the two spectra obtained from the even and odd samples in the two-phase polyphase decomposition of the original sequence. The polyphase spectra are obtained as follows. The echo sequence consists of complex-valued time series where each resolution volume is represented by N complex samples. This sequence of N samples is split into two subsequences containing the samples with even and with odd time indices. Three spectra are then estimated: 1) the spectrum of the even-index samples, 2) the spectrum of the odd-index samples, and 3) the spectrum of the overall original sequence. The $\phi_{DP\text{-}EO}$ is then computed and thresholding is applied to identify Doppler velocity bins where the intrinsic $\phi_{DP\text{-}EO}$ is nearly zero. For such bins, the spectral coefficients of the power spectrum are very likely GC contributions. Simulation examples in Section 3 illustrate this phenomenon. The power spectrum coefficients identified as GC are then notched from the original spectrum. The notched void can be "repaired" using either linear interpolation or a Gaussian fit. The moments are obtained from the censored spectrum. We leave the void in this paper because we wish to visually assess our identification scheme. Optional adjustment of the spectral noise level at the locations with strong GC contributions can be used to reduce GC residuals due to raised spectral skirts (Bachmann and Zrnic 2007). The new method is summarized as follows, where IQ [1×M] is a complex-valued time series acquired from some particular resolution volume:

1. Estimate the total power – mean($|IQ|^2$).
2. Remove *dc*
3. Split the IQ vector into even and odd indexed polyphases: IQ_{even}=IQ(2m) and IQ_{odd}=IQ(2m+1), 0 ≤ m ≤ M/2.
4. Apply window
   - Rectangular for total power P < 20 dB,
   - Blackman for 20dB < P < 80 dB,
   - Blackman-Nuttal for P > 80 dB.
5. Estimate the three spectra for the original, even and odd sequences S [1×M], S_{even} [1×M/2], and S_{odd} [1×M/2] respectively.
6. Optionally estimate the mean noise from the rank order statistics on S and adjust the noise level.
7. Use the complex spectral coefficients of S_{even} and S_{odd} to find the $\phi_{DP\text{-}EO}$ = arg($S_{even}S^*_{odd}$), where "*" indicates complex conjugation.
8. Construct spectral mask:
$$\text{MASK}= \begin{cases} 1, & |\phi_{DP\text{-}EO}|<0.1^\circ \\ 0, & \text{otherwise.} \end{cases}$$
9. Apply this mask to the original spectrum S to notch the clutter spectral coefficients and use linear interpolation to repair the void if desired.
10. Estimate the spectral moments.

For a mechanically steered antenna, the $\phi_{DP\text{-}EO}$ is not zero precisely. Nonetheless, the method can be used with rotating antennas. For that, the angle threshold for the mask (step 7 above) should be larger. The new angle threshold will depend on the speed of rotation and the number of pulses (spectral coefficients).

3. SIMULATIONS

Fig. 1a shows Doppler spectra for 100 realizations of a signal containing weather and clutter and simulated with the following parameters: pulse repetition time PRT=0.8 ms, signal to noise ratio SNR=20 dB, clutter to signal ratio CSR=40 dB, spectral width of σ_v =2 m s^{-1}, and radial velocity of weather v=10 m s^{-1}. The corresponding $\phi_{DP\text{-}EO}$ (Fig. 1b) has a reduced maximum unambiguous velocity (v_a), namely v_a/2.

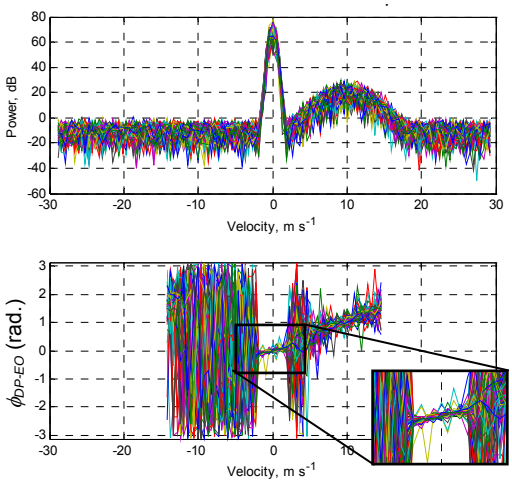

Fig.1. a) Doppler spectra and a) $\phi_{DP\text{-}EO}$ for 100 realizations of signal simulated with PRT=0.8 ms, SNR=20 dB, CSR=40 dB, σ_{vc}=0.28 m s^{-1}, σ_v =2 m s^{-1}, v=10 m s^{-1}.

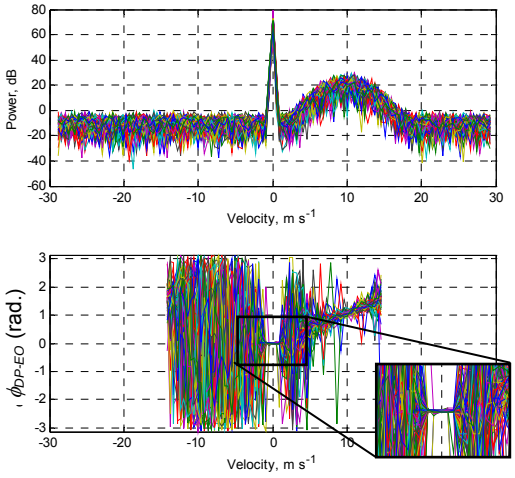

Fig.2. a) Doppler spectra and a) $\phi_{DP\text{-}EO}$ for 100 realizations of signal simulated with PRT=0.8 ms, SNR=20 dB, CSR=40 dB, σ_{vc}=0.1 m s^{-1}, σ_v =2 m s^{-1}, v=10 m s^{-1}.

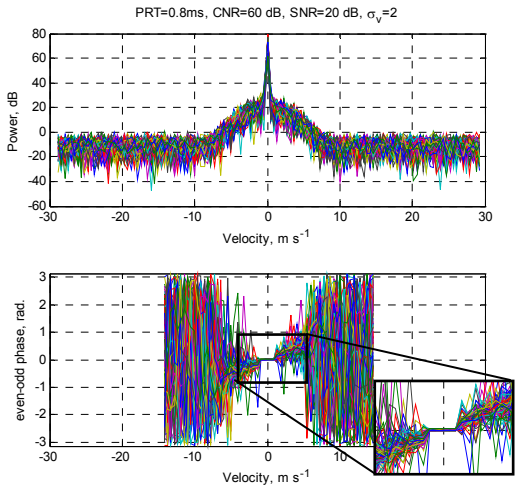

Fig.3. a) Doppler spectra and a) $\phi_{DP\text{-}EO}$ for 100 realizations of signal simulated with PRT=0.8 ms, SNR=20 dB, CSR=40 dB, σ_{vc}=0.28 m s^{-1}, σ_v =2 m s^{-1}, v=0 m s^{-1}.

This is not a concern, because for the GC identification, only the small velocity values are needed. Fig. 1b shows that the phase does not significantly change at the Doppler bins with clutter, changes randomly at the Doppler bins with noise, and exhibits fluctuations at the Doppler bins with weather. The value σ_{vc}=0.28 m s^{-1} for spectral width of clutter accounts for the smearing due to the antenna rotation. This simulation is representative of spectra obtained from a mechanically steered antenna. Note that there is a slope in the $\phi_{DP\text{-}EO}$ at the Doppler velocities corresponding to GC (Fig.1b, zoomed inset).

Fig. 2 shows spectra and the $\phi_{DP\text{-}EO}$ for the same simulation parameters except σ_{vc}=0.1 m s^{-1}. This example is representative of spectra acquired using an electronically steered antenna. The flat portion (Fig. 2b zoomed inset) indicates the GC spectral coefficients. Fig. 3 depicts a situation where clutter and weather peaks collocate in the Doppler spectrum. Clutter can be recognized by the flat portion in the $\phi_{DP\text{-}EO}$ (Fig. 3b zoomed inset).

Figs. 4a-c show a field of Doppler spectra simulated for 100 different weather velocities in the interval between -5 m s^{-1} and 5 m s^{-1} with SNR=40dB and GC with SNR=40dB. Small velocities are chosen to ensure overlap of weather spectra with the clutter spectra. Figs. 4a and 4b show the unfiltered spectra and the spectra with the notched clutter contribution respectively. The color bar indicates the power in a logarithmic scale. Fig. 4c depicts the $\phi_{DP\text{-}EO}$ field. The color bar shows the phase in radians. The phase is noisy at the locations on the Doppler fields with low power. There is a direct correspondence between the phase and the radial velocity. The phase reflects the difference in the Doppler shifts between adjacent spectral coefficients. Figs. 4d-f show simulations of similar to Figs 4a-c situation without ground clutter. Clutter filter is applied everywhere, however only a few spectral coefficients (white dots) are filtered. These simulations indicate that the $\phi_{DP\text{-}EO}$ is a powerful new tool for spectral clutter identification.

4. RADAR AND DATA COLLECTION

Data were collected with the S-band phased array radar at the National Weather Radar Testbed (NWRT), which is maintained and operated by the National Severe Storm Laboratory (NSSL) in Norman, Oklahoma. The radar covered a northern 90° sector between 315° and 45° in azimuth, at elevation 0.5°.

The data sets were collected
in clear air on
July 26, 2007, at 13:32 UTC, and
July 30, 2007, at 15:50 UTC, and
in precipitation on
Sept. 19, 2007, at 13:46 UTC and
Sept. 25, 2007, at 13:50 and 15:14 UTC.

The pulse repetition time was 0.8 ms resulting in a maximum unambiguous velocity of 31.25 m s^{-1}. The range resolution was 60 m. The angular resolution was 1 degree. The number of pulses per resolution volume was 128, allowing spectral resolution of approximately 0.5 m s^{-1}. The radar scanned a sector of the atmosphere in consecutive radials analogous to the data acquisition scheme of mechanically steered radar.

5. SPECTRAL CLUTTER IDENTIFICATION

Fig. 5 shows an example of GCF in spectral fields with storms. The radial is from 20° azimuth observed on Sept. 25, 2007. The axes are range from the radar and Doppler velocity. Note that range starts from 10 km due to the physical limitation of the NWRT at this time (2007). The original spectrum (Fig. 5a) mainly consists of signatures from GC, direct current *dc*, three portions of storms, and clear-air. The GC contributions are visible at ranges below 25 km. The *dc* component is a temporary glitch in the radar hardware that appears in the spectrum as a steady line at zero Doppler velocity and at all ranges. The storms visible in the spectral field are at ranges of about 20 km, between 35 and 50 km, and beyond 90 km. These storms stand out as clusters with large powers. The filtered spectral field (Fig. 5b) shows that the GC and *dc* are successfully removed. A Blackman and Blackman-Nuttal windows were used to reduce leakage of strong clutter components into the weaker weather component. The noise floor was leveled and the ground clutter was notched. The $\phi_{DP\text{-}EO}$ (Fig. 5c) shows zero phases at the points corresponding to the Doppler velocity near zero.

Fig. 6 shows an example of GCF in spectral fields with clear air. The radial is from azimuth 333° on July 26, 2007. The unfiltered spectra (Fig. 6a) contain strong signatures from GC, *dc*, and a weak clear-air contribution. This is a challenging exercise for clutter filtering because the clear-air signals are weak and

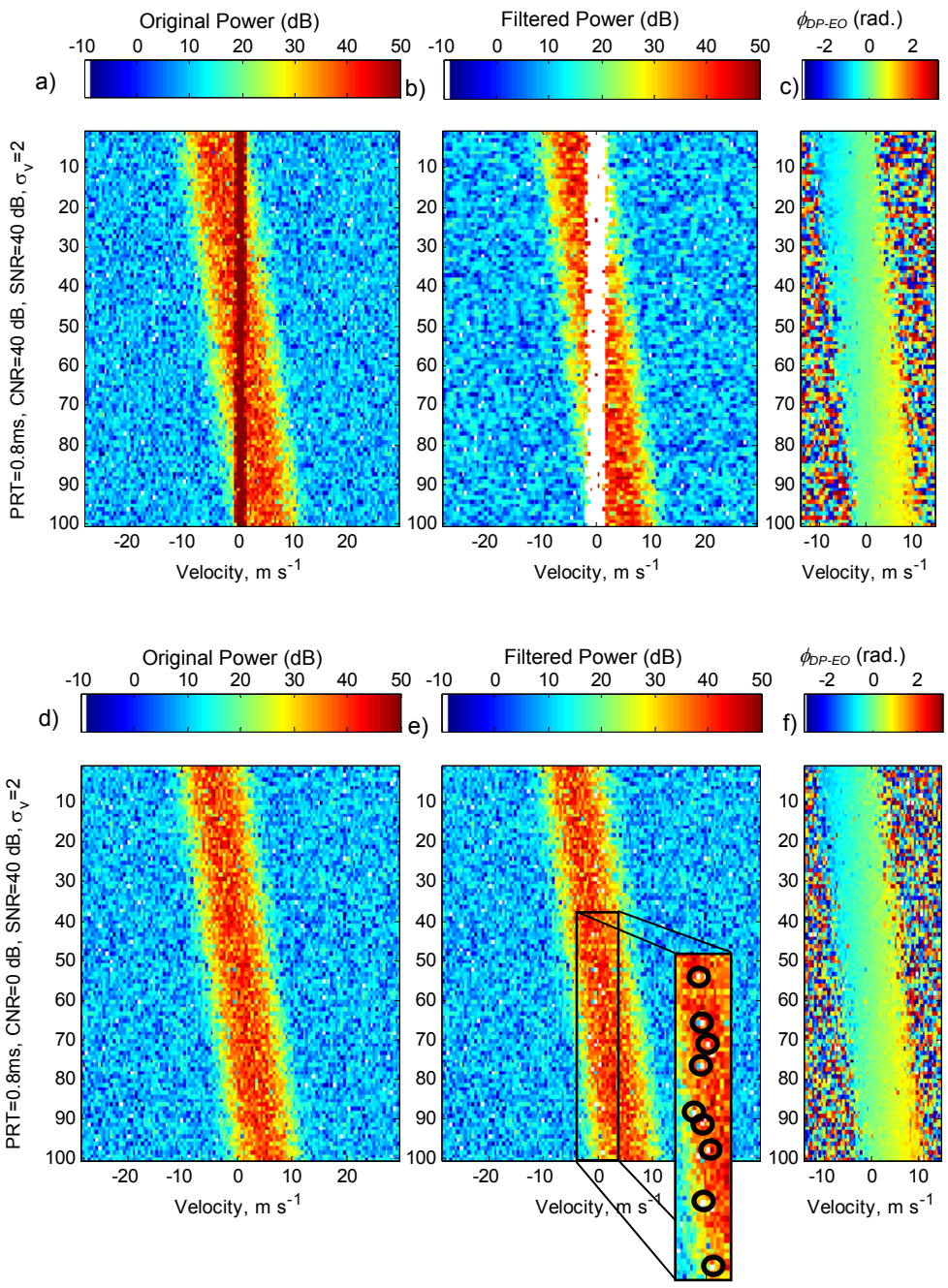

Fig. 4. Illustration of clutter filtering for spectral fields simulated with clutter (a-c) and without clutter (d-f): a,d) unfiltered power spectral density, b,e) filtered power spectral density, and c,f) ϕ_{DP-EO}. The simulation parameters are PRT=0.8ms, SNR=40 dB, σ_{vc}= 0.28 m s^{-1}, and σ_v =2 m s^{-1}, v=-5:0.1:5 m s^{-1}, a-c) CNR=40dB, and d-f) CNR=0dB.

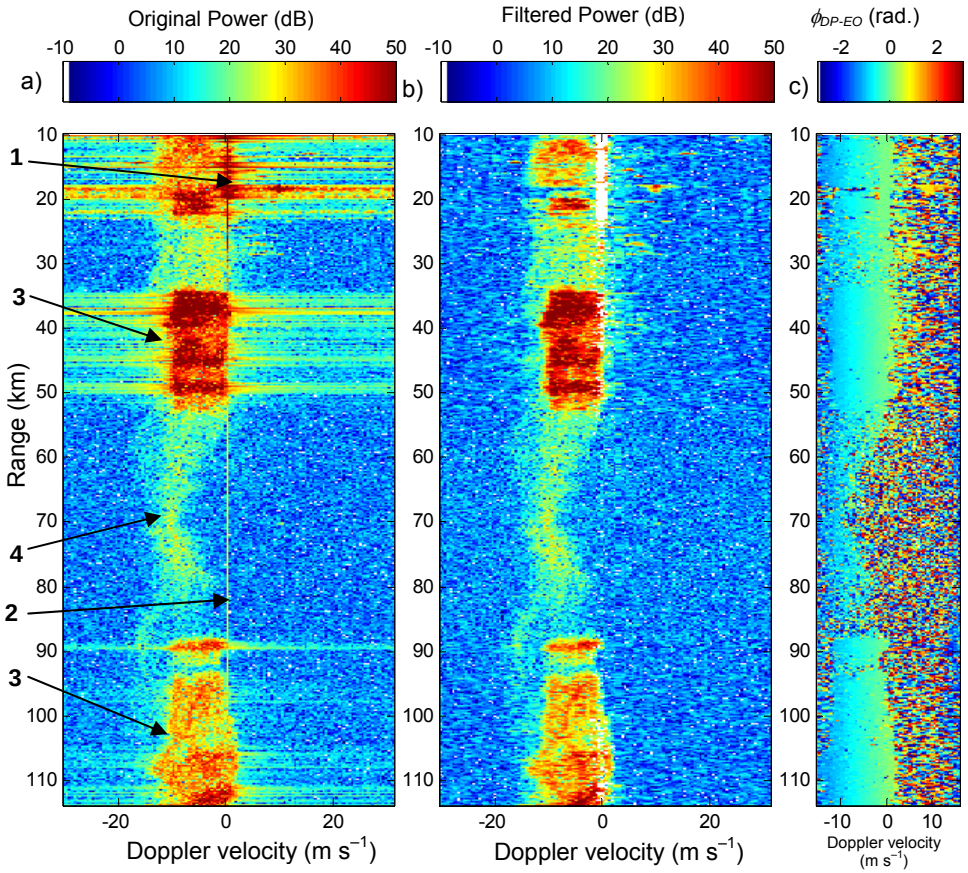

Fig. 5. The fields of a) the unfiltered power spectral density, b) the filtered power spectral density, and c) ϕ_{DP-EO}. Data are from Sept. 25 2007, 15:14 UTC, azimuth 20°. Arrows indicate: 1 - ground clutter; 2 – *dc*; 3 – storms, and 4 – clear-air signature. The original spectrum is weighted with the rectangular window. The filtered spectrum is weighted with Blackman, Blackman-Nuttal and rectangular windows depending on power.

located at zero Doppler velocity. The spectral field with identified and notched GC contributions (Fig. 6b) shows the de-cluttered clear-air signal. The spectral coefficients identified as ground clutter are removed aggressively by our proposed algorithm, but not so aggressively that we destroy the constructive signal components. Note that the ϕ_{DP-EO} provides a non-symmetric clutter recognition strategy to remove GC and *dc* and preserve, for the most part, the weak clear-air signal.

Fig. 7 shows the spectral fields along a radial at azimuth 6° from storms observed on September 25, 2007. The original spectrum (Fig. 7a) contains strong signatures from storms and GC. We have side knowledge that the ground clutter is absent between 110 km and 120 km from other observation sources. Nonetheless, the spectrum with notched GC contributions (Fig. 7b) shows that several spectral coefficients within the storm signature are notched. This is due to the *dc* component and due to mistaking the storm coefficients with GC. In any case, the number of spectral coefficients identified as clutter is small and a simple linear interpolation over the gap can recover a possible loss of power. The GC and *dc* are successfully identified over the entire radial.

6. RADAR MOMENTS

Plane position indicators (PPI) of the Doppler moments are shown in Figs. 8-9 for two cases, in precipitation and in clear air respectively. The unfiltered PPIs are presented in the left column. The filtered PPIs are shown in the right column. Clear air power exposes the GC pattern (Fig. 9a) that is also recognizable in precipitation (Fig. 8a). The zoomed insets of power PPIs in Figs. 8a-b and 9a-b clearly show that GC is filtered and the remaining echoes are exposed. The velocity PPIs (Figs. 8c and 9c) of unfiltered data show a large area with zero velocities due to *dc*. Filtered velocities (Figs. 8d and 9d) show areas with speckled velocity values. These are the areas with insignificant echo power that are generally hidden behind the thresholds. We do not threshold PPIs because we wish to expose, observe and compare all echoes. Thresholding can be applied later on. The PPIs of spectral width (Figs. 8e and 9e) show that GC echoes have characteristic small values

of spectral width. These disappear after filtering (Figs. 8f and 9f). The regions with insignificant power expose large values of spectral width that are further increased after filtering. Two more examples of clutter filtering are given in Fig. 10. Figs. 10a and 10b show unfiltered/filtered powers for a clear-air case that occurred on July 30, 2007, at 15:50:10 UTC. Figs. 10c and 10d show unfiltered/filtered powers for a precipitation case that occurred on September 25, 2007, at 15:14:52 UTC. Figs. 10e and 10f show unfiltered/filtered powers for a precipitation case that occurred on September 9, 2007, at 13:46:46 UTC. These examples provide evidence that the GC is removed and the weather signals are preserved. Fig. 10e is an example of unusual GC pattern due to abnormal beam propagation. Note that even though a simple notch was used for filtering, there is no evidence of the zero isodop. In applications where it is desirable to do so, a simple interpolation may be applied to the spectral coefficients adjacent to the notch to provide additional power if the zero isodop is observed. However, interpolation was not used for the examples shown in this paper; rather, power was estimated from the spectral coefficients remaining after the notch.

7. CONCLUSIONS

We presented a powerful new spectral methodology for ground clutter identification that overcomes the limitations associated with static clutter maps. This totally new approach can be used to adaptively filter ground clutter from the radar data acquired with electronically or with mechanically steered radars. We use the phase rather than the power of the complex radar signal for identification. We presented clutter filtering results for the National Weather Radar Testbed phased array radar in clear air conditions and in precipitation. The technique does not require clutter maps and can successfully remove intrinsic ground clutter contributions while preserving weather contributions to the Doppler spectrum.

8. REFERENCES

Bachmann, S., and D. Zrnić, 2007: Suppression of Clutter Residue in Weather Radar Reveals Birds' Corridors over Urban Area. *Geoscience and Remote Sensing Letters*, IEEE, to appear.

Golden, J., 2005: Clutter mitigation in weather radar systems filter design & analysis. *System Theory, SSST '05. Proc. 37th Southeastern Symposium on*, 386 – 390.

Hubbert , J.C., M. Dixon, and C. Kessinger, Real time clutter identification and mitigation for NEXRAD. AMS, 5B.6. Available at ams.confex.com/ams/pdfpapers/117270.pdf

Ice, R.L., D. A. Warde, A. D. Free, R. D. Rhoton, D. S. Saxion, C. A. Ray, N. K. Patel, O. E. Boydstun, D. S. Berkowitz, J. N. Chrisman, J. C. Hubbert, C. J. Kessinger, M. Dixon, and S. M. Torres, 2007: Optimizing clutter filtering in the WSR-88D. *23rd Conf. on IIPS*, American Meteorological Society, P2.11.

Siggia A. D., and R. E. Passarelli, Jr, 2004: Gaussian Model Adaptive Processing (GMAP) for improved ground clutter cancellation and moment calculation. *Proceedings of ERAD (2004)*, Copernicus GmblH, 67-73.

Torres, S., 1998: Ground Clutter Canceling with a Regression Filter, NOAA/NSSL Report, 37 pp.

U.S. Department of Commerce/NOAA, *Federal meteorological handbook #11: Doppler radar meteorological observations. Part C. WSR-88D products and algorithms*, FCM-H11C-2006.

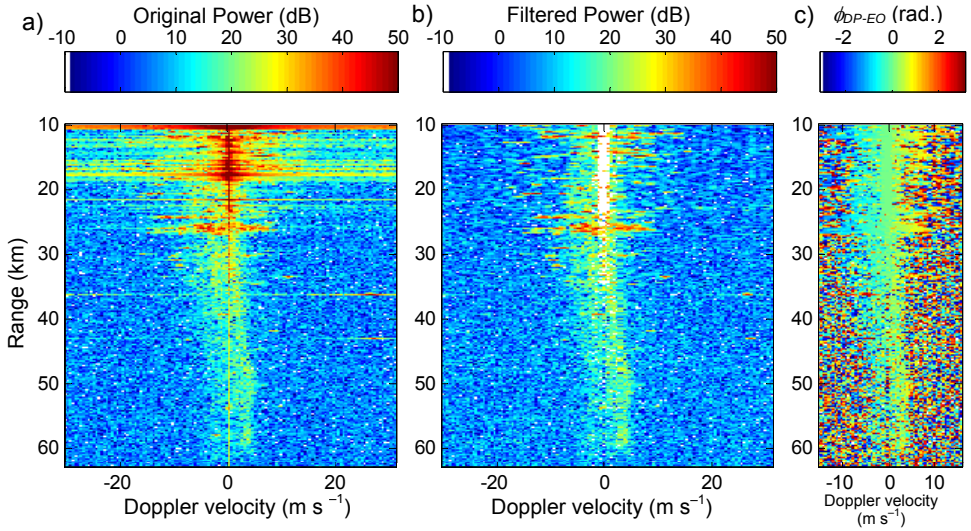

Fig. 6. Spectral fields for clear air a) the unfiltered power spectra, b) the filtered power spectra, and c) ϕ_{DP-EO}. Data are from July 26 2007, 13:32 UTC, azimuth 333°.

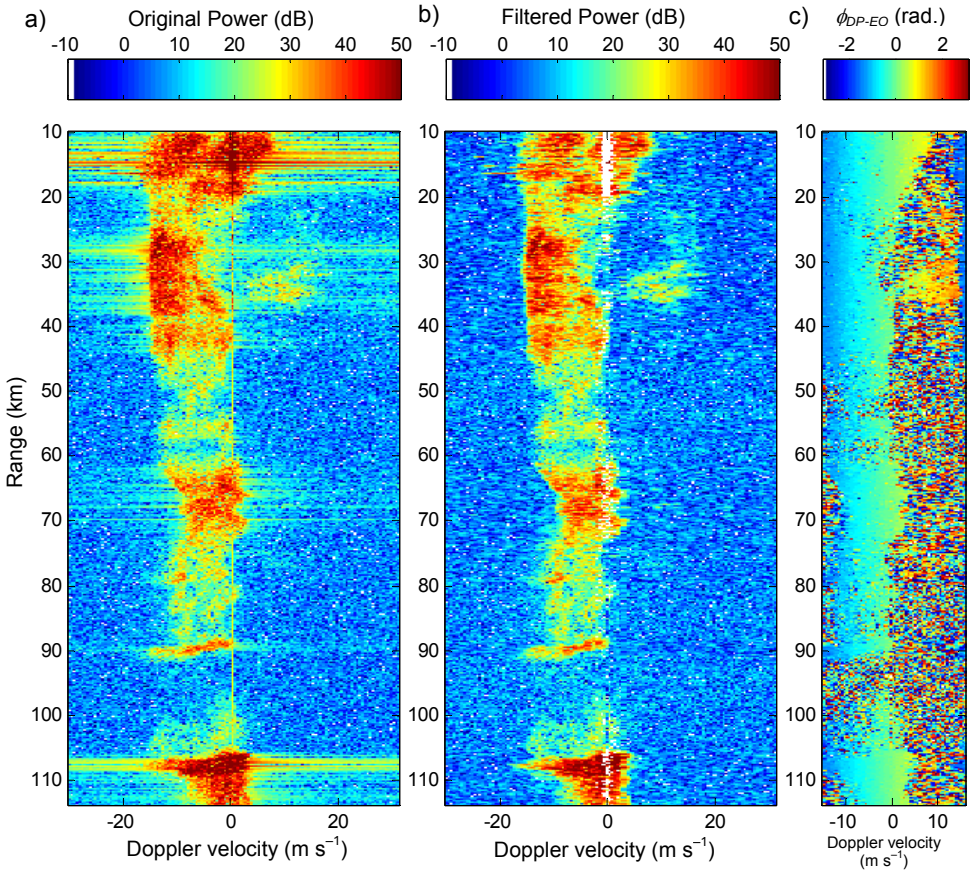

Fig. 7. Spectral densities for precipitation a) the unfiltered power spectra, b) the filtered power spectra, and c) ϕ_{DP-EO}. Data are from Sept. 25 2007, 13:49 UTC, azimuth 6°.

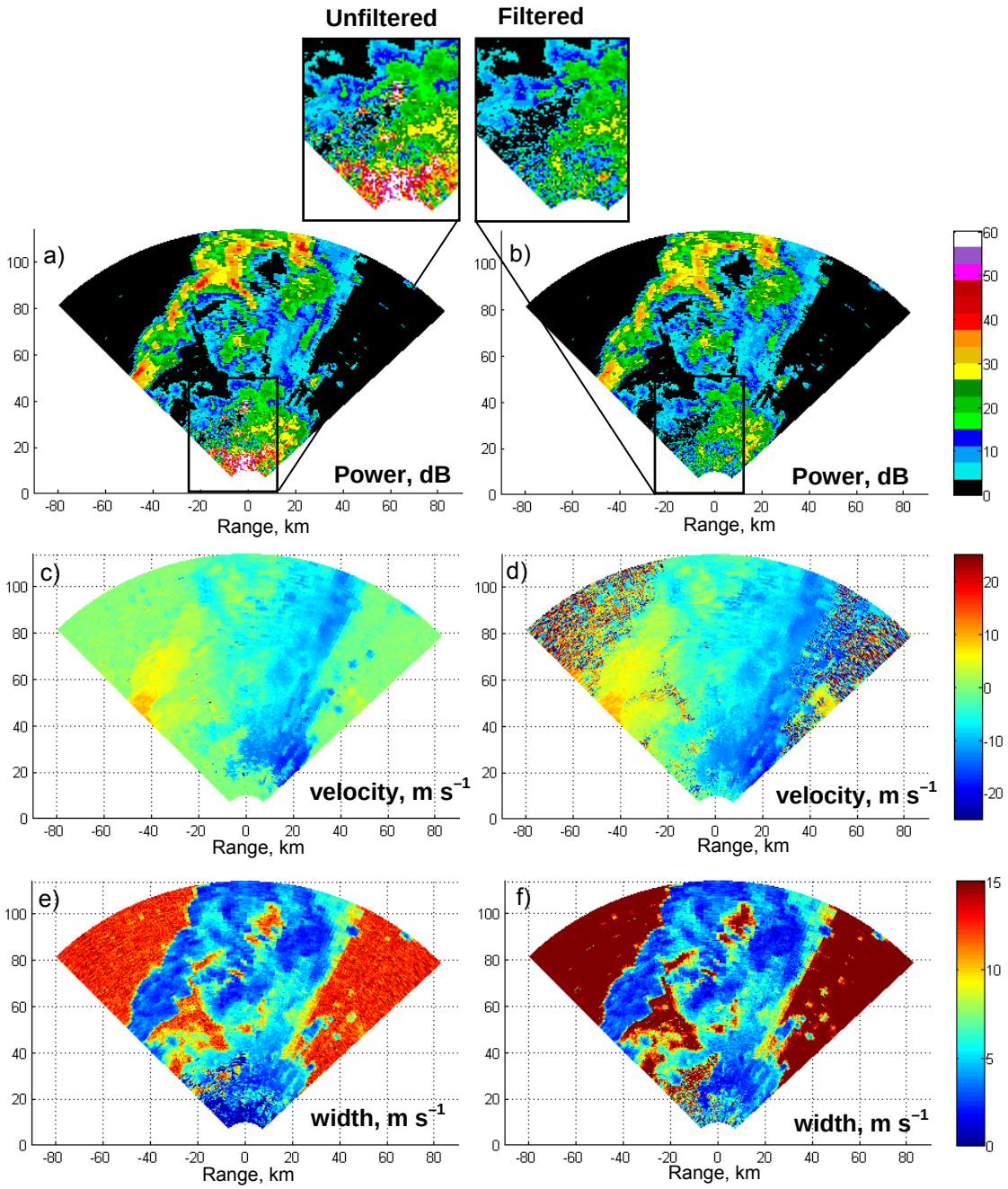

Fig. 8. Examples of PPIs with storms: unfiltered (left) and filtered (right): powers (top), velocities (middle) and spectral widths (bottom). Data are from Sept. 25, 2007, 13:49 UTC.

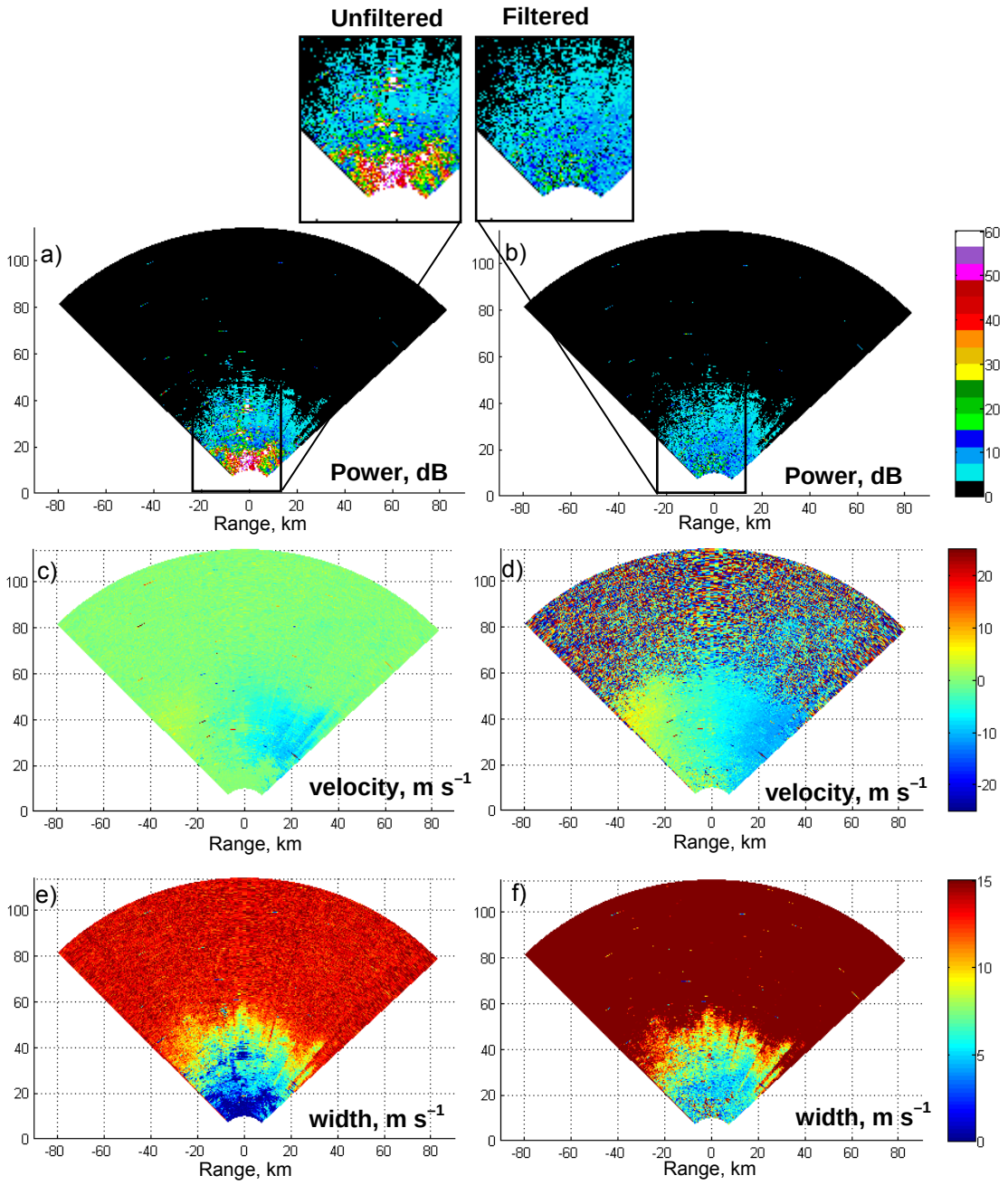

Fig. 9. Examples of PPIs with clear air: unfiltered (top) and filtered (bottom) powers(left), velocities(middle) and spectral widths(right). Data are from July 26, 2007, 13:32 UTC.

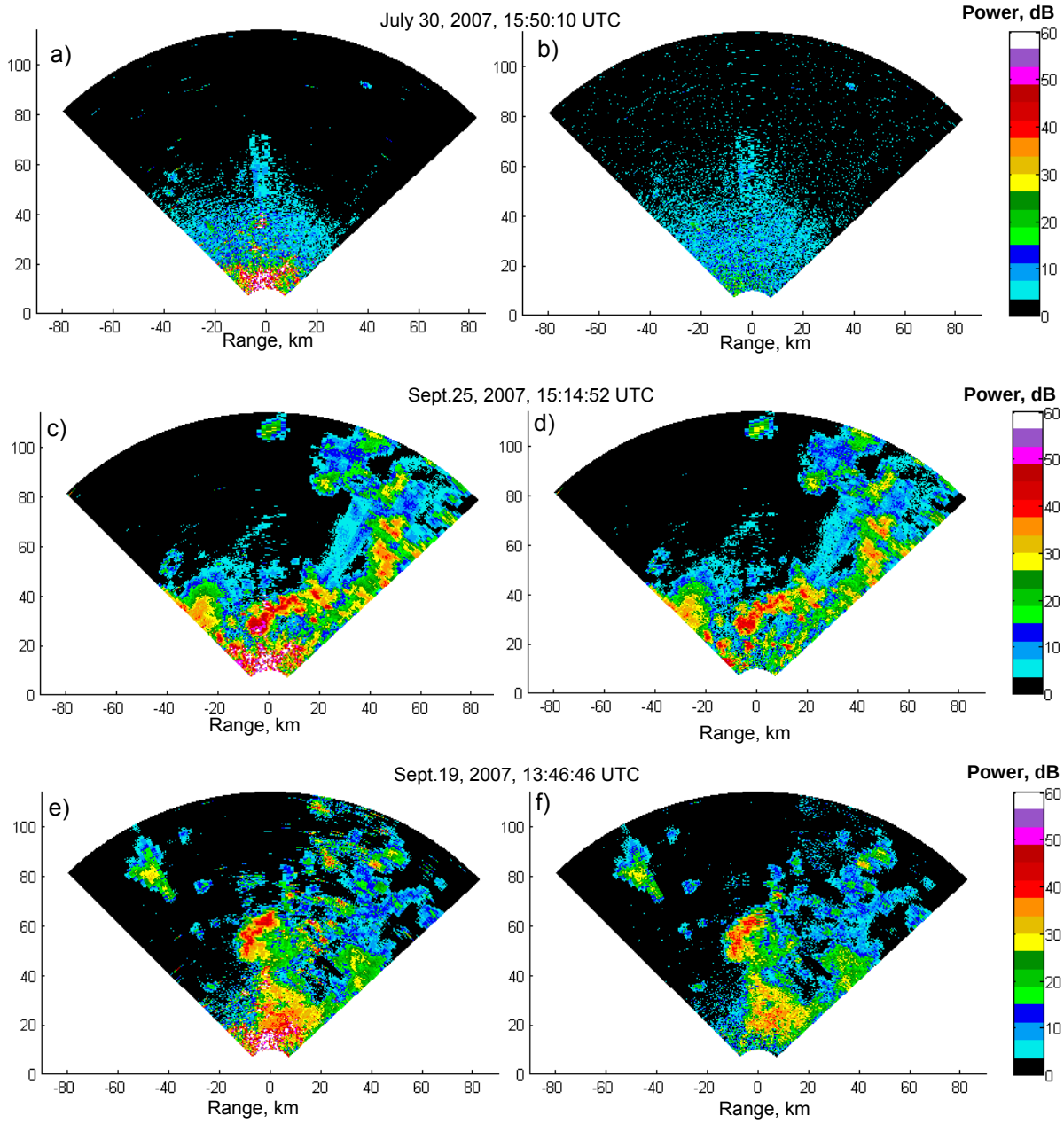

Fig. 10. Displays depict the unfiltered power (left) and power after proposed GCF (right) for clear air (top) and precipitation (middle and bottom) cases. The identified clutter was notched.